ChemComm

Accepted Manuscript

This is an *Accepted Manuscript*, which has been through the Royal Society of Chemistry peer review process and has been accepted for publication.

Accepted Manuscripts are published online shortly after acceptance, before technical editing, formatting and proof reading. Using this free service, authors can make their results available to the community, in citable form, before we publish the edited article. We will replace this *Accepted Manuscript* with the edited and formatted *Advance Article* as soon as it is available.

You can find more information about *Accepted Manuscripts* in the **Information for Authors**.

Please note that technical editing may introduce minor changes to the text and/or graphics, which may alter content. The journal's standard **Terms & Conditions** and the **Ethical guidelines** still apply. In no event shall the Royal Society of Chemistry be held responsible for any errors or omissions in this *Accepted Manuscript* or any consequences arising from the use of any information it contains.

Chemical Communication

INVITED FEATURE ARTICLE

Advances of the environmental transmission electron microscope (ETEM) for nanoscale *in situ* studies of gas-solid interactions.

J.R. Jinschek,[a]

Although available since the early days of electron microscopy, recent technology developments of the environmental transmission electron microscope (ETEM) have enabled new research in the study of nanomaterials in gaseous environments. Significant improvements in scanning / transmission electron microscope (S/TEM) technologies, while containing a gaseous environment close to the object under investigation, enable now atomic scale study of phenomena occurring during gas-solid interactions. A focus behind these developments is the research on nanomaterial-based technologies, for instance for efficient energy conversion, use and storage as wells as for environmental protection. *In situ* high spatial resolution characterization provides unique information that is beneficial for understanding the relationship between structure, property and function of nanostructures directly on their characteristic length scales.

The progress in recent research is reviewed to highlight the potential of the state-of-the-art differentially-pumped microscope platform, based on the latest microscope generation optimized for atomic scale *in situ* investigations. Using cases from current catalysis research, high resolution imaging reveals structural changes in nanocatalysts when being active and is instrumental in understanding deactivation processes; while spectroscopy gives additional access to reactivity. Also, imaging schemes are discussed that focus on enhancing the achievable imaging resolution, while having the effect of electron beam / solid interaction in the nanomaterial under control.

1. Introduction

The development of better technologies for efficient use of our natural resources, for efficient energy conversion, for efficient transportation, for food production, for environmental protection, etc. relies heavily on advances in developing new and improved nanostructures and nanomaterials. Characterization on the (sub-)nanometer length scale, focusing on structural evolution with the link to the nanomaterial's 'performance', plays a crucial role for obtaining detailed knowledge about the relationship between structure, unique property and function in these systems of reduced dimensions. Fortunately, atomic-scale scanning/ transmission electron microscopy (S/TEM), significantly enhanced by recent advancements, [1,2] has become a powerful and indispensable tool for nanomaterial characterization [3] with spatial resolution in the sub-nm range, with energy resolution in the sub-eV range, and with sensitivity to detect single atoms (see Fig 1).[4] S/TEM provides a unique ability to image size, shape, bulk/surface/interface structures of individual nano-objects and

measure electronic properties as well as elemental distributions at these small length scales.
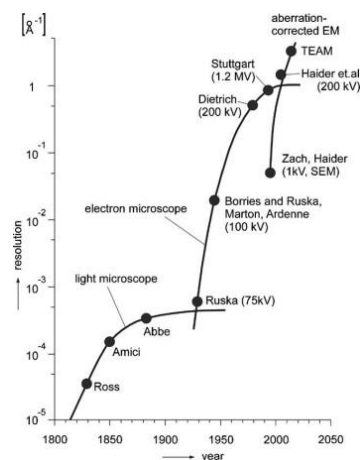

Fig. 1 Improvement in imaging resolution of the microscope over the last decades.[4] Aberration corrected EM represents a significant improvement in imaging resolution and sensitivity.

Focusing on nanomaterial's application in gaseous environments in nature and in technology, many phenomena occur during gas–solid interaction with significant impact on the nanostructure's properties and performance. However, the dynamic state of nanomaterials 'in operation' can't always be inferred from examination under high vacuum conditions or from postmortem studies. For instance, the state of a heterogeneous catalyst and the catalyst's properties are intimately dependent on the reaction environment. [5] Direct observations under operating conditions are therefore of utmost importance.

In situ characterization techniques enable visualization of structural evolutions in functional nanomaterials under (near) operational or environmental conditions. These investigations offer essential insights related to questions about the structural integrity of nanostructures when 'at work'. This is applied in a wide field of applications in fundamental and applied research focusing on gas-solid interactions, e.g. oxidation, reduction, catalysis, crystal growth, gas storage and filtering, corrosion and its prevention, just to name a few. For instance in case of a catalyst, it adds insights to unveil the relationship between nanostructure and catalytic performance (activity, stability, selectivity, etc.). Although an arsenal of *in situ* imaging and spectroscopic techniques, [6] e.g. using photons at various wave-lengths (e.g. visible, infrared, X-rays and gamma-rays) are beneficially applied, the information is averaged over length scales larger than the characteristic dimensions of the nanostructure itself, whereby detailed information about morphologies as well as surface and interface structures in the nanomaterials are left uncovered. In contrast, *in situ* S/TEM studies [7] offer a visualization of atoms in real space and time and are therefore an essential complement to these other key techniques. [8]

Applying atomic-scale S/TEM techniques in *in situ* studies of gas-solid interactions is, however, extremely demanding. Using accelerated electrons for imaging and spectroscopy requires high vacuum conditions in essential segments of the electron microscope column to avoid compromising the high resolution imaging and analytical capabilities. A key challenge for establishing environmental conditions inside an electron microscope is to confine gas environments in the close vicinity of the specimen while maintaining the microscope's overall performance and stability.

Here, the focus of the article is on the concept of achieving such a gaseous environment confinement by a differentially pumped vacuum system, generally referred as an environmental scanning/ transmission electron microscope (ETEM). After a brief reminder of the history, the article focuses on some recent application examples highlighting the potential of the latest ETEM generations (e.g. FEI Titan ETEM G2) [9] based on the high performance microscope generation. [10] It will be concluded by a discussion on the aspects that generally play a role when imaging sensitive nanomaterials. It is essential to understand and control electron beam / material interactions by selecting the right imaging conditions in order to observe structural evolutions inherently relevant to the technical use of the nanomaterial.

2. Brief synopsis about development of differentially pumped ETEM

Since the invention of the transmission electron microscope (TEM), [11] technology developments have been focused not only on improving the microscope performance in terms of resolution (Fig. 1) and sensitivity, but also on confining the high vacuum requirements only to microscope parts essential for beam generation and data capture, thereby allowing a gaseous and reactive environment to be introduced around the object under investigation (E. Ruska in 1942, Fig. 2). [12,13]
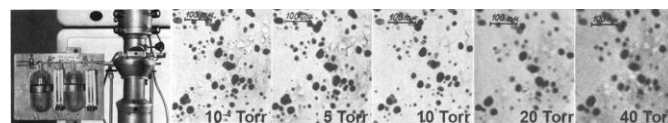

Fig. 2 Left: Device for gas supply on the early transmission electron microscope "Übermikroskop" in 1942. Imaging example: Colloidal silver particles observed under increasing air pressure. [12]

Essentially, two technologies for environment confinement have emerged over the years, as reviewed earlier. [14-16] One is utilizing the concept of differentially evacuating individual vacuum stages of the microscope column separated by additional small pumping apertures. [17-21] This allows large pressure differences Δp ($\Delta p \geq$ nine orders of magnitude) between specimen area and an electron source requiring high vacuum conditions with an otherwise free 'line of sight' for the electron beam. The other approach is using additional, electron-transparent 'windows' to confine a gaseous environment close to a specimen. [22,23] Here, additional interaction between window material and electron beam, gaseous environment, as well as specimen might need to be considered.

Currently, application of a microscope with differentially pumped vacuum system seems more widespread, most likely due to its robustness and compatibility to specimen types as well as flexibility in experimental conditions. In particular, the use of standard TEM specimen holders support various sample geometries and might even enable additional (*in situ*) functionality, such as for tomography, for optical studies (e.g. of photocatalysts) or for mechanical testing (e.g. of metals).

Environmental transmission electron microscopy techniques, often abbreviated as ETEM, E-TEM, ESTEM, E-S/TEM, etc. and sometimes also referred to as controlled atmosphere or environmental-cell TEMs, have enabled essential *in situ* studies on nanostructures. This review focuses on some recent applications enabled by advances of differentially pumped ETEM.

There is a growing list of surveys about historical aspects and advances in differentially-pumped ETEMs, e.g. [14-16,19,20,24-26] In essence, over the decades there have always been successful approaches to incorporate gas confinement into the then present microscope generation, mainly to benefit from the enhancements in imaging and spectroscopy capabilities. [12,13,16-21,27-29] Earlier

approaches have been based on prototype 'environmental cells'. Today's solution (Fig. 3) is based on a unique intimate integration of differential pumping stages already in the beam forming objective lens, e.g. Boyes et al. [17] This concept minimizes the impact on the underlying state-of-the-art electron microscope's capabilities in terms of imaging and spectroscopic functionality. [30]

The major improvement in electron microscopy in the last one and a half decades (see time line in Fig 1) has been the implementation of new hardware components such as correctors compensating for aberrations present in the probe forming lens [1,2] and monochromators minimizing the energy spread in the primary electron beam. [31,32]
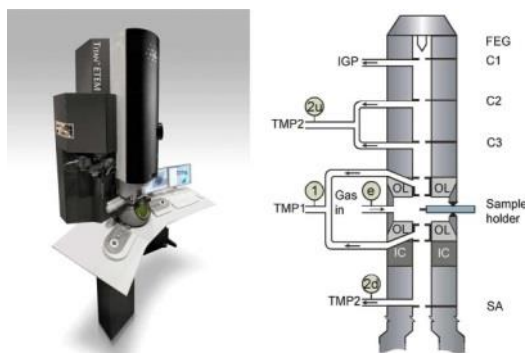

Fig. 3 Differentially pumped environmental transmission electron microscope (ETEM – here a FEI Titan ETEM G2, [9,30] including a sketch of the vacuum system highlighting the pressure-limiting apertures at the stages of the objective lens (OL), the condenser lenses (first (C1), second (C2) and third (C3)) and the selected area (SA) aperture (details in ref 30).

These technological breakthroughs are nowadays incorporated in the state-of-the-art ETEMs as well. [20,21,30] Such ETEMs are thus equipped with a (high-brightness) field-emission gun, [33] a gun monochromator, [31,32] an aberration corrector, [1] an energy filter for imaging and electron energy loss spectroscopy (EELS), [18] an energy dispersive X-ray spectrometer (EDS), scanning capabilities for STEM & bright-field/dark-field detectors, [16,34] digital cameras, which all are mounted on a mechanical, electronic and thermal stable microscope. Build on a high performance microscope platform, [10] FEI's Titan ETEM G2 (Fig. 3) [9] atomic-resolution S/TEM is an all-in-one solution for standard high vacuum applications and for time-resolved *in situ* studies of nanomaterials during exposure to gaseous environments. The software-controlled user interface offers a range of settings to accommodate both handling by novice (automatic mode) as well as advanced (manual control) operators. Gas pressures in ETEM experiments can be accurately preset from 10^{-3} Pa up to 2000 Pa (limits in case of nitrogen gas N_2). It is equipped with a mass spectrometer to determine gas composition either in the gas inlet system or in the specimen area. A built-in plasma cleaner allows for cleaning of the specimen area after using a gas. For safe and reliable use the Titan ETEM G2 features built-in hardware and software protections. [8]

3. Application examples

A limited selection of ETEM applications in various fields of research has been chosen to illustrate the advances in ETEM capabilities in terms of imaging and spectroscopy of solid materials in gaseous environments. Thereby it highlights how ETEM technology advances have enabled new essential structural information that are beneficial to improve our understanding of nanomaterials' structure-property-function relationships. For a more thorough overview of published applications the author refers to a collected list @ FEI.com/ETEM. [9,35,36]

3.1. Study size, shape and structure changes of catalyst nanoparticles in operational conditions

Nearly 90% of all chemical processes in industry are based on catalysis. It is therefore indispensable to develop a fundamental understanding of the functionality of catalysts. Properties of catalytically active nanoparticles (e.g. activity, selectivity, stability) are directly related to their size, shape and structure. [5] *In situ* atomic scale structural observations are therefore inadmissible for understanding the catalyst's structure-function relationship because under its reactive conditions the catalyst may undergo significant changes to become active. The need for understanding a catalyst's active state and stability has been one of the strong driving forces for improving ETEM capabilities and functionality over the years.

Earlier differentially pumped ETEM versions already enabled *in situ* S/TEM with increasing imaging performance to follow structural developments of catalysts under (near) reaction conditions. [19,37-46] Hansen et al. [42] have reported high resolution images of copper (Cu) nanocrystals that are active as catalysts in methanol synthesis and hydrocarbon conversion processes. Figure 4, *in situ* high-resolution TEM images showing an imaging resolution below 0.2nm, depicts the dynamic reversible shape changes of the nanocatalyst caused by changes in the gaseous environment. [42]
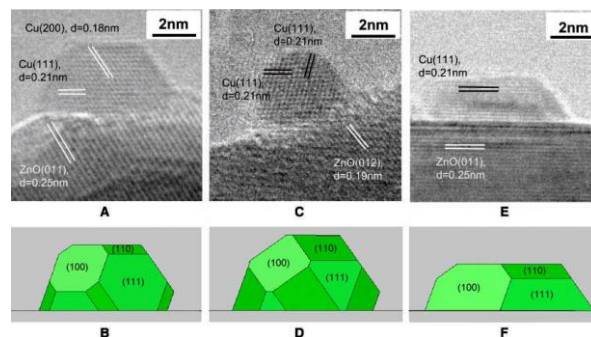

Fig. 4 *In situ* TEM images (A, C, and E) showing the reversible shape changes of a copper (Cu) catalyst on zinc oxide (ZnO) support in various gas environments together with the corresponding Wulff constructions of the Cu nanocrystals (B, D, and F). (A) The image was recorded at a pressure of 1.5 mbar of H_2 at 220°C. (C) Obtained in a gas mixture of H_2 and H_2O, $H_2:H_2O = 3:1$ at a total pressure of 1.5 mbar at 220°C. (E) Obtained in a gas mixture of H_2 (95%) and CO (5%) at a total pressure of 5 mbar at 220°C. [42]

This finding, imaging *in situ* individual nanoparticles, confirms earlier experimental evidence for reversible morphology changes in small metallic Cu particles in this high surface area, porous catalyst system, e.g. using *in situ* extended x-ray absorption fine structure (EXAFS). [47] However, the *in situ* TEM sets apart from those previous studies by allowing quantitative identification of the catalytic important crystal facets of the Cu nanoparticle and their gas-dependent abundance to be obtained. Moreover, this dynamic shape change is governed by adsorbate-induced changes in surface and interface energies and emphasizes that the active state of a catalyst is strictly speaking only present during catalysis.

As indicated before, one of the major improvements in electron microscopy has been the implementation of correctors compensating imaging lens' aberrations; thereby minimizing contrast delocalization and providing 'sharp images' of nanostructures, especially their surfaces and interfaces. [1] Using an aberration corrector on ETEM should further strengthen the interplay between *in situ* TEM and established surface science approaches. This great potential, without imposing the traditional 'materials gap', has been already shown when revealing active catalyst's surface sites and adsorbed product species on a catalyst surface at the atomic scale. [48]

Insight in the role of surface sites on catalytic activity can also be obtained from – combining *ex situ* electron microscopy, density functional theory (DFT) calculations, and EXAFS measurements. [49] Building on this approach, Cargnello et al. [50] recently investigated the direct relationships between structure and function on metal catalysts supported on ceria (CeO₂). Varying the length of the metal-support interface they found that CO oxidation in ceria-based catalysts is enhanced at the ceria-metal interface sites (for group VIII metal catalysts). [50]
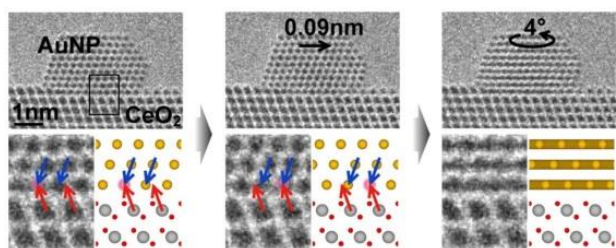
Fig. 5 Atomic scale *in situ* HRTEM study of gold (Au) nanoparticles supported on CeO₂, an active catalyst for carbon monoxide (CO) oxidation at low temperatures. In reaction environment for CO oxidation Au nanoparticles move reversibly and stepwise by approximately 0.09 nm on the CeO₂ support surface. The lateral displacements and rotations occur back and forth between equivalent sites. [53]

In case of gold (Au) nanoparticles, an active catalyst for carbon monoxide (CO) oxidation at low temperatures when supported on CeO₂, atomic scale *in situ* studies directly reveal structural changes of the Au/CeO₂ catalyst under reaction conditions. [21,45,51-53] Kuwauchi et al. [53] have shown that the catalytically active Au nanoparticles move reversibly and stepwise on the CeO₂ support surface, as indicated in Figure 5. Au catalysts are used for CO oxidation in a partial pressure range of one 1 Pa to 10 Pa, and the catalytic activity is proportional to the partial

pressure of CO, even at pressures below 10 Pa. For *in situ* experiments, a gas composition of 1vol% of CO in air at 45-100Pa has therefore been applied to mimic environmental conditions. [21,52,53] Au nanoparticles translate back and forth between equivalent sites by lateral movements of about 0.09 nm and by rotations of about 4 degrees, indicating that Au nanoparticles migrate on the surface with low activation energy. Kuwauchi et al. [53] have suggested that the Au nanoparticles are likely anchored to oxygen-deficient sites on the CeO₂ surface. The perimeter interfaces between nanocatalyst and support, the most probable activation sites, are structurally not rigid. [53] This work illustrates that *in situ* TEM is also suitable for addressing the complex metal-support interface in catalysts.

Aberration corrected imaging is furthermore beneficial to retrieve the surface structure of nanoparticle catalysts. For example, the structure of the Au {100} surface develops to form an Au{100}-hex reconstructed surface structure under reaction conditions. [52] The average distance of adjoining Au atomic columns on the {100} surface facet has changed. Prior and subsequent observations in high vacuum conditions show the nominal Au {100} surface. Although larger-scale surface reconstructions on catalysts have been reported before using *ex situ* TEM, [54] there is no guarantee that the state of reactive surface is maintained during transfer and for such dynamic surface it is vital to establish a direct, atomic scale visualization of the surface morphology on catalysts in working state as demonstrated by figures 4 and 5. Interestingly, Yoshida et al. [52] also observed a densely packed phase of CO molecules adsorbed at the on-top sites of the Au atoms in the well-extended reconstructed {100} facets, confirmed by image simulations based on DFT calculations (see Fig. 6). [52] This may give hope that gas-surface interactions can be furthered detailed on nanometer-sized particles.
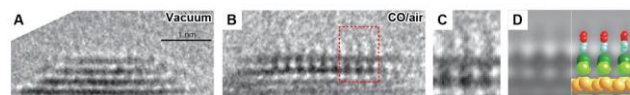
Fig. 6 Atomic scale *in situ* HRTEM images of the Au {100} surface visualizing adsorbed CO molecules on a Au{100}-hex reconstructed surface under catalytic conditions, (A) in vacuum and (B) in reaction environment (1 volume % CO in air at 100 Pa at room temperature). (C) The observed image in the rectangular region in (B) at higher magnification. (D) A simulated image based on an energetically favourable model. The model is superimposed on the simulated image. [52]

An energy filter for EELS had been already incorporated in ETEMs in the 1990s. [18] The 'window free' ETEM design based on a differentially pumped column vacuum system seems beneficial for *in situ* EELS investigations by avoiding having electron beam interaction with window material.

These spectroscopy capabilities have opened one path to link observed structural information of nanocatalysts with measurements of their reactivity (structure-function relationship) - an important step in catalysis research.

Wang et al. [55] have followed the dynamic redox process taking place in individual ceria zirconia nanoparticles. Those particles

are a critical component in automotive three-way catalytic converters and have potential applications in areas, where redox functionality is important. *In situ* EELS studies indicate considerable variability in redox activity (oxidation states) and *in situ* nanoscale imaging correlates these to structural and compositional information. [55]

EELS has also been used for analysis of gas-characteristic fingerprints in a spectrum to determine gas composition *in situ*. [56] By using a special catalyst loading, this methodology proved sufficiently sensitive to quantify gaseous reaction products in an ETEM. [57] Thus, by combined TEM-EELS measurements, Chenna et al. [57] have opened up a possibility to combine structural characterization of a working catalyst with simultaneous measurements of its activity (Fig 7).
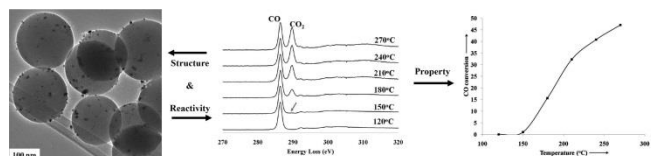

Fig. 7 Demonstration of reaction products in an ETEM correlating catalyst structure and reactivity.
left: in situ TEM image of 2.5 wt % Ru/SiO$_2$ catalyst under reaction conditions
center: Background subtracted *in situ* EELS spectra acquired at different temperatures during CO oxidation on Ru/SiO$_2$ catalyst.
right: Diagram showing the CO conversion rate vs. increase in temperature directly derived from the *in situ* EELS measurements. [57]

3.2. Studies to understand catalyst's deactivation by coke formation

Another ongoing aspect in catalyst R&D is to develop a detailed understanding on improving stability of a catalyst e.g. by preventing sintering effects [58-62] or by blocking active sites with poisons and by-products in the chemical reaction (for example by coverage with carbon, as reported e.g. here [29,48,63-67]).

Understanding this carbon coverage ('coke formation') is essential to develop strategies to prevent poisoning of catalysts used, for example, for synthesis gas production. These studies on 'filamentous carbon formation' (graphene, nanotubes and nanofibres), e.g. catalysed by different metal particles when exposed to acetylene, have been pioneered by Baker et al. [29,63] It has been found that acetylene decomposition is taking place on surface facets that develop under catalytic working conditions. From time-resolved TEM, the growth kinetics was evaluated and an apparent activation energy barrier was obtained. As the energy barrier matched carbon diffusion barriers in bulk metals, the main rate-determining step for carbon deposition was proposed to be carbon diffusion through the catalyst particle. [63]
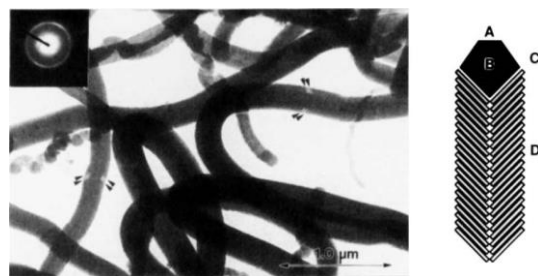

Fig. 8 *In situ* TEM micrograph of carbon filaments produced from the reaction of a C$_2$H$_2$/H$_2$ (1:4) mixture with platinum black at 550 °C. Stacking of the carbon is indicated by lines and arrows.
right: Schematic representation of a carbon filament produced from the metal-catalyzed decomposition of a hydrocarbon: (A) metal-gas interface, (B) metal catalyst particle, (C) metal-carbon interface, and (D) ordered platelets of carbon produced by precipitation of carbon from the metal particle B. [64]

Figure 8 depicts results from *in situ* experiments that have been focused on formation of carbon deposits resulting from decomposition of ethylene and acetylene on platinum (Pt). [64]
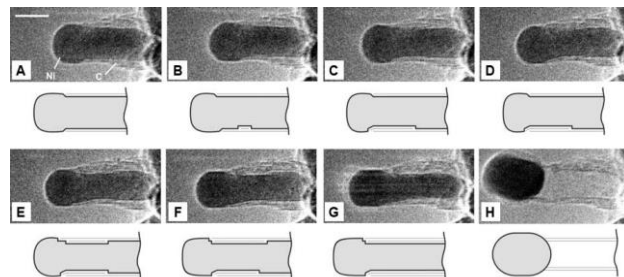

Fig. 9 *In situ* TEM image sequence of a growing carbon nanofibre (CNF), acquired *in situ* with CH$_4$:H$_2$ = 1:1 at a total pressure of 2.1 mbar with the sample heated to 536 °C.
Images A–H illustrate the elongation/contraction process. Corresponding schematic drawings are included to indicate mono-atomic Ni step edges at the C–Ni interface. Scale bar is 5 nm. [48]

To address the surface processes involved in nanofiber growth, Helveg et al. [48] utilized high-resolution *in situ* TEM methods (Fig. 9) to study the formation of carbon nanofibre (CNF) - from decomposition of methane on nickel (Ni) nanocatalysts (CH$_4$ → C (solid) + 2H$_2$). The experimental conditions have been a gas mixture of CH$_4$:H$_2$ = 1:1 at a total pressure of ~ 200Pa and a temperature of 500–540°C, carefully chosen to balance the pressure ratio of the oxidizing and reducing component in the chemical potential term of $\Delta G = \Delta G^0 - kT \ln(p_{CH4}/p_{H2}^2) \approx 0$. [48] In this case the metal surface should play a more specific role for the growth. [68] Time-resolved *in situ* TEM was used to monitor Ni surface sites in action and how adsorbed carbon species form. Nucleation of graphene happens at mono-atomic step edges on the catalyst surface with a carbon nanostructure growth mechanism involving surface diffusion of C and Ni atoms, as consistently confirmed by DFT calculations. [48,69] These results demonstrate that ETEM is beneficially applied in combination with surface science methods to pinpoint structure-sensitive reactivity of surface sites.
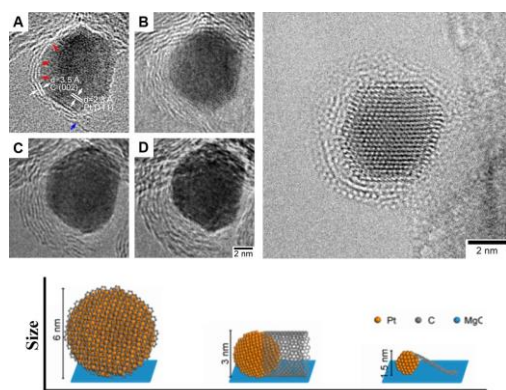
Fig. 10 HRTEM imaging to study formation of graphene layers on MgO-supported Pt nanoparticle.

left: time-lapsed *in situ* HRTEM images of the growing graphene layers on Pt recorded under exposure of 1.3 mbar iso-butene at 475 °C (A: 0 s; B: 1 s; C: 1.2 min; and D: 3.2 min), taken with an electron dose of 1.5×10^5 e$^-$/nm^{2}s.

right: ex situ HRTEM image of the grown graphene layers on Pt after being exposed under 1.3 mbar iso-butene for 60 min at 475 °C in the *in situ* experiment, taken with an electron dose of 7.8×10^4 e$^-$/nm^2.

bottom: Schematic representation: Pt particles with ø > 6 nm develop a complete particle envelopment with grapheme layers. At Pt particles with ø < 6 nm, carbon nanotubes develop or graphene sheets move from the surface of the Pt particles. [67]

By using *in situ* and *ex situ* HRTEM imaging, Peng et al. [67] have studied the formation of graphene layers on MgO-supported Pt nanoparticle widely used to catalyze transformation of alkanes, e.g. by dehydrogenation. Also in this case, HRTEM images indicate that graphene sheets grow from steps on the surface of the catalyst nanoparticle (Fig. 10). It has been found that the morphology of the developing carbon nanostructures is strongly particle-size dependent (see lower part in Fig 10). [67]
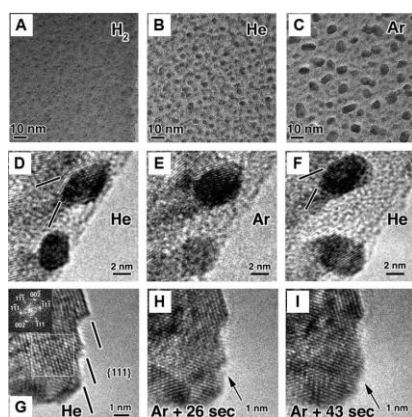

Fig. 11 *In situ* TEM of Fe catalyst as a function of gas environment. (A to C) Size evolution of Fe catalysts after 60 min under H$_2$ (A), He (B), and Ar (C) at 500°C and 500 mtorr. (D to F) Series of images from the same two Fe catalyst particles held at 500°C, as the gas overpressure is changed from (D) 500 mtorr He to (E) 500 mtorr Ar to (F) 500 mtorr He. (G to I) Series of images from a larger Fe catalyst particle along a 110 zone axis. (G) Image taken in 500 mtorr He at 500°C, showing very strong {111} facets. (H) After the introduction of Ar, local degradation of the facets begins. (I) With further time at 500°C in the Ar environment, the facet has been completely removed. For all cases, the H$_2$O with base pressure of 10^{-2} mtorr is present. Arrows in (H) and (I) indicate the gradual defaceting features over time. [71]

Currently, there is also a large interest in growing different allotropes of carbon on the nanoscale. Such carbon formation studies have been extended to investigate different stages in growth of carbon nanotubes (CNT) with targeted properties or CNT stability in gaseous environments, e.g. reported here. [65,66,70-74] For example, Harutyunyan et al. [71] have demonstrated a correlation between nanocatalyst morphology and the resulting CNT electronic structure. *In situ* TEM studies revealed that varying the gas environment during thermal annealing of the catalyst leads to differences in morphology and coarsening behaviour of the nanoparticles (Fig. 11) favouring nucleation of CNT with metallic conductivity by chiral-selective growth. [71] Kim et al. [72] have utilized quantitative measurements of CNT growth rates and (*in situ*) observations, and have showed that termination of CNT array growth is in fact linked to evolution of catalyst's morphology as for the CNF already shown in figure 9.
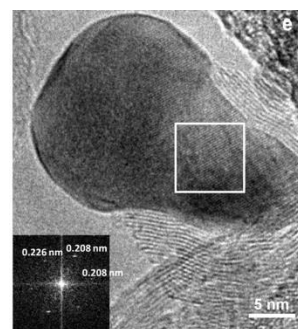

Fig. 12 *In situ* HRTEM image of formation of carbon nanostructures on Au-Ni/SiO$_2$. The FFT pattern (inset, taken from the boxed area in the TEM image) confirms bulk diffusion of carbon by indicating a Ni$_3$C structure in the catalyst particle. [66]

In another example, Sharma et al. [66] have investigated the role of added Au atoms in the Ni nanocatalyst in terms of formation of carbon nanostructures, such as CNT or CNF. Single-walled CNTs have been formed at temperatures above 600°C in samples doped with less than 0.2 mol fraction of Au. DFT calculations confirm that the addition of a mol fraction of Au enhances the carbon diffusion through the bulk of the particle (Fig. 12). Thus, Au substation apparently modifies the microscopic mechanisms to influence morphology and yield of the CNT structures. [66]

Recently, Koh et al. [75] have performed *in situ* oxidation studies on CNT. Despite the expected higher energy of the atoms at the CNT cap, the oxidation appears at the outer side wall first with indications that 'imperfections' in the structure are the starting point (Fig. 13). Also, it was found that CNTs with a number of walls greater than six are more resistant to oxidation. [75]
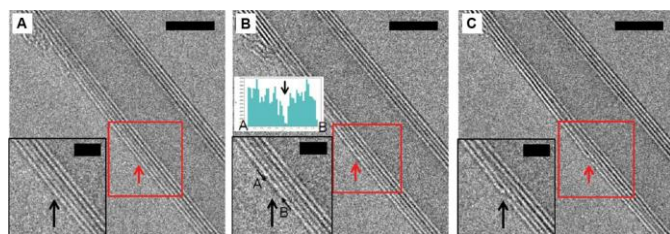
Fig. 13 Aberration-corrected *in situ* TEM images showing the structural changes in a CNT after being exposed to a heated, oxygen (O_2) environment. Observations of a possible initiation site for outer wall oxidation. (A-C) Images of the same nanotube at 400 °C, at 400 °C after 1.5 mbar oxidation, and at 520 °C after 1.5 mbar oxidation, respectively. The red arrow in (B) shows a darker image spot, which appears to be the initiation site for oxidation (red arrow in (C)). The insets are higher-magnification images of the areas indicated by the red boxes. The line profile taken along 'A-B' (inset of (B)) is shown above its inset, where the arrow corresponds to the darker image spot. Scale bars in (A) to (C) represent 5 nm. Scale bars in the insets represent 2 nm. [75]

3.3. Study photocatalysts – need of light in *in situ* gas experiments

Since the environmental cell is an integral part of a differentially pumped ETEM, the microscope itself maintains flexibility in terms of enabling additional *in situ* functionality, such as for studies that require the exposure of nanomaterials to (sun)light. This enables, for instance, studies on photocatalytic nanomaterial that are relevant for sustainable energy research. Cavalca et al. [76] have developed a prototype TEM specimen holder for *in situ* illumination to study light-induced phenomena in photoactive materials and photocatalysts under working conditions, e.g. photodeposition of Pt onto a GaN:ZnO photocatalyst (see Fig 14). [76]
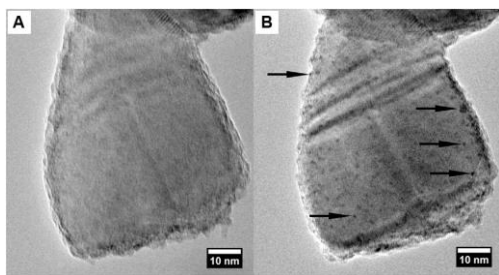

Fig. 14 *In situ* TEM of light-induced photocatalytic reactions. Here: bright-field TEM images of a GaN:ZnO particle (A) before and (B) after reaction in 5 mbar H_2O and with 6 W cm^{-2} light at 405 nm wavelength. The arrows in (B) show some of the deposited Pt nanoparticles. [76]

Further, photoreduction of cuprous oxide (Cu_2O) has been studied. [77] Cu_2O is a working photocatalyst for hydrogen evolution but it photocorrodes when exposed to light illumination in an aqueous environment. Such *in situ* studies are essential for further material optimization. [77]

Miller et al. [78] have developed a prototype optical fibre system with a high intensity broadband light source with high illumination intensity. [78] Water splitting conditions (light illumination in aqueous environment) have then been realized in an ETEM for characterizations of the surface structure of anatase nanocrystals. [79] *In situ* experiments have been performed without simultaneous sample illumination by the

electron beam to prevent its impact. It has been found that the initially crystalline surface converts to an amorphous phase with a thickness of up to two monolayers of titanium in a different oxidation state (Fig 15). This stable, heavily hydroxylated amorphous surface layer seems to be relevant to photocatalytic splitting of water. [79]
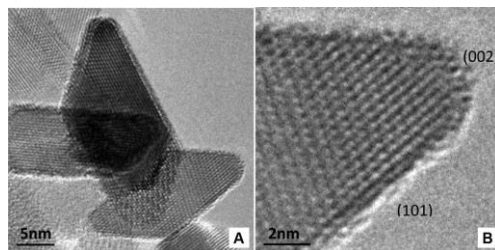

Fig. 15 *In situ* TEM of light-induced photocatalytic reactions. Here: water splitting conditions for characterizing surface structure evolution of anatase nanocrystals *In situ* HRTEM images of (A) fresh anatase particles after 40 h in H_2O gas at 150 °C, light exposure 12 h; (B) magnified images of the (101) and (002) surfaces after illumination. [79]

4. How to achieve atomic scale resolution in *in situ* experiments?

The selection of application examples above has been used to highlight that atomic scale information of functional nanostructures and -materials are of paramount importance. Over the last decades, atomic-scale S/TEM has become a crucial tool to provide such information. In terms of imaging performance, high-resolution S/TEM at ≤0.1nm resolution typically requires high vacuum at ≤10^{-5} Pa, electron energy E of 300 keV, and a beam intensity (or electron dose rate, dD/dt) on the specimen of ~10^5 - 10^6 e$^-$/nm^2 s.

These electron dose rates can be argued for by following the reasoning introduced by A. Rose, [80,81] who stated that a certain signal-to-noise ratio (SNR_{Rose}) is necessary to be able to distinguish image features with a certain confidence. The attainable imaging resolution d is determined not only by the microscope resolution d_{TEM} but rather by a convolution of d_{TEM} and the accumulated electron dose D on the image forming detector:

$$d = \sqrt{d_{TEM}^2 + \frac{(SNR_{Rose})^2}{C^2 D}} \qquad (1)^{80,82}$$

Using this relationship, the *Rose criterion* $SNR_{Rose} \geq 5$ and $C = 1/e^2$ (~0.14), as the criterion for necessary contrast to discriminate, one can estimate the required accumulated dose D to distinguish atomic scale features in the image. In dynamic experiments this particular dose would be required in any chosen time frame to maintain atomic resolution, i.e. the corresponding electron dose rate or equivalently brightness β of the microscope's electron source must have a certain level. As an example, brightness values β achieved by FEI's high-brightness XFEG^{TM} [33] should theoretically enable such high resolution imaging conditions even with 100s of frames per second. However, the electron illumination conditions for high

resolution S/TEM imaging could be unsuitable for studying functional nanomaterials, because these structures might be affected by the interaction with the electron beam. Functional nanomaterials, such as catalyst, are high surface area materials consisting of atomic arrangements (surfaces, interfaces) with lower bond energies compared to bulk. Thus, to observe dynamics inherently reflecting the experiment as such and to maintain the potential of comparing *in situ* TEM results with information achieved from other *in situ* experiments as well as data from *ex situ* or post mortem investigations, structural reorganization caused by electron beam need to be avoided or at least be controlled and specified.

It is generally acknowledged that the nanostructures are affected by knock-on collisions and ionization effects (radiolysis) under electron illumination. [83] These effects depend in general dependence on the chosen energy of the electrons impinging on the specimen. Using the flexibility in state-of-the-art instrumentation, a careful choice of the incident electron beam energy can be beneficial to minimize knock-on collision. For example, knock-on collisions are the dominating interaction effect for electrical conductive materials and low energy imaging conditions below the knock-on threshold value have been chosen for investigations of carbon nanomaterials (e.g. of graphene [84]). But lowering the beam energy may be disadvantageous for electrical insulating materials for which an increasing contribution of ionization effects may obscure atomic scale observations. [83] Thus, varying-voltage S/TEM techniques might in some cases not be sufficient to minimize beam/sample interactions.

In the presence of gaseous environments, electron beam interactions have been studied [14,15,85,86] and are still the focus of on-going investigations. [30,87-90] Due to the extended gas phase in the differential pumping system, part of the electrons, scattered elastically and inelastically on the specimen and gas phase, will thereby follow trajectories through the microscope's imaging system that prevent contribution to the constructive image formation (reduced signal S), or they follow trajectories that do not focus into the image plane of the microscope so an effective contribution to the image noise level N is obtained. [87-89] Moreover, gas molecules are typically light elements and so enhanced ionization effects may result in invasive influence of the electron beam on the dynamic processes under inspection. A comparison to experiments with the beam blinded off in-between the initial and the final stage ("beam off") would give indications about its influence on the experimental results. [76,79]

Thus, in light of this discussion, one has to carefully balance between resolution and sensitivity in *in situ* TEM experiments. In addition to optimizing the microscope's optical settings, achieving highest imaging resolution will be specimen- and gas-dependent (gas type and pressure). Recent advances in instrumentation and methodology seems to open up for two new possible routes for optimizing the imaging schemes applies in *in situ* TEM experiments. According to equation (1), one should be able to improve the *in situ* imaging resolution d

(i) by improving the contrast C. [82] With the advent of aberration corrected HRTEM imaging, contrast improvements

can be done using the negative contrast mode (NCSI). [90] This method yields images of atomic columns in nanostructures as bright spots on a uniform background noise level. [82,91]

(ii) by accumulating the electron dose D in the image using lower electron dose rate conditions but with a corresponding longer acquisition time. [92-95] In this weak excitation approach [93] the average time between successively delivered electrons are increased to allow electron-induced specimen excitations to vanish such that the alternations in the electrostatic potential of the specimen is recovered. [95,96] Single weakly-bound atoms on nanocatalyst surfaces have been resolved under high vacuum conditions with this imaging scheme. [95] Such sophisticated imaging schemes are readily applicable for *in situ* observations, both using TEM and STEM, but require drift corrected frame imaging (e.g. DCFI) and will be just limited by characteristic time-scale for the specimen dynamics.
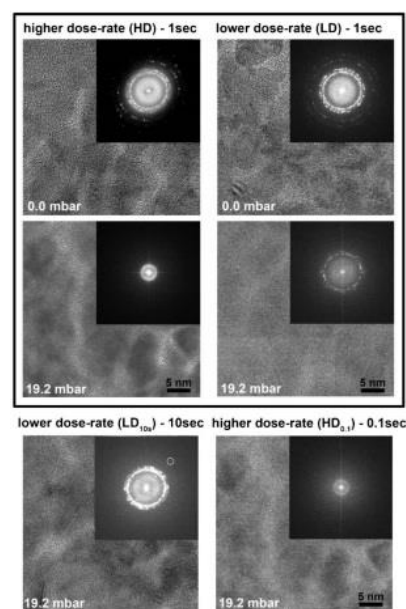

Fig. 16 Investigation of achievable resolution in imaging in gas environments under different electron dose rate conditions.

In situ HRTEM images of the Au/C specimen with corresponding FFT displays inserted. The HRTEM images were acquired *in situ* with a 300 keV electron beam during the exposure to 0.0 and 19.2 mbar N_2 under the higher dose-rate (10^6 e^-/nm^2 s) and the lower dose rate (10^5 e^-/nm^2 s) conditions. All four upper images (in frame) were acquired with the same 1 s exposure time resulting in a total dose = 10^6 e^-/nm^2 (left column) and a total dose = 10^5 e^-/nm^2 (right column). Additional micrographs (below frame), taken under the LD condition with 10 s exposure time as well as the HD condition with 0.1 s exposure time, highlight the difference in achievable resolution in images acquired with the same total dose of 10^6 e^-/nm^2 (left column) and of 10^5 e^-/nm^2 (right column) but under different dose-rate conditions. The scale bar is 5 nm in all images. [30]

The latter scenario of applying low electron dose rates has indeed been proven beneficial in *in situ* imaging in gaseous environment. [30] A considerable improvement in imaging resolution was demonstrated using lower dose rate conditions of 10^5 e^-/nm^2s and longer exposure time of 10 seconds than higher dose rate conditions of 10^6 e^-/nm^2s for corresponding shorter exposure time of 1 second to fulfil the *Rose criterion*. [30] In fact, using the low dose rate illumination conditions, the

inherent 0.10 nm resolution of the Titan ETEM was shown to be retained for gas pressures up of 1000 Pa and with only a slight resolution deterioration to 0.12 nm resolution obtained in 2000 Pa N_2 environment (see Fig. 16). [30] This indicates that the imaging performance of state-of-the-art ETEMs are not chromatically limited but rather determined by the combined probe/gas/sample interactions, which necessitates lower dose rate conditions for exploiting non-invasive high resolution imaging.

Here the author would like to highlight some examples of experimental procedures that have been applied to quantify effects of beam/sample interactions and enabling observations under conditions where the effect of the electron beam is negligible.

First, improving *SNR* (and thereby the achieved imaging resolution) in *in situ* observations has already been demonstrated by drift-corrected frame-averaged summation of successively recorded TEM images under lower electron dose rate conditions. [52,58] In a study of nanoparticle sintering, the structural changes were systematically mapped out under varying electron dose rates. By applying a back-extrapolation principle, a time-window and low electron dose rate was identified under which the observed nanoparticle sintering process was concluded to be thermally induced and the electron beam effect far less than the actual pixel size. [58]

Second, when investigating ceria-catalyzed oxidation of soot in relation to diesel engine emission control, Simonsen et al. [97] observed a beam-enhanced shrinkage and quantitatively found by varying the beam intensity that an electron dose rate $< 10^4$ e^-/nm^2s during *in situ* imaging was sufficient to avoid beam effects on the soot particles. Under those conditions, resolution was limited to the nanometer scale due to the limited *SNR*. This approach enabled a quantitative comparison of the soot oxidation kinetics observed in the *in situ* TEM experiment and in *ex situ* reactor experiments which substantiated the direct visualization that catalytic soot oxidation involves reaction centres at the soot–CeO_2 interface. [97]

Third, Kuwauchi et al. [46] have investigated dose rate effects on titania (TiO_2) support for catalytic Au nanoparticles. Under electron beam irradiation TiO_2 is more fragile than other supports, as for instance CeO_2. Fig. 17 shows typical structural reorganization processes in Au/TiO_2 under electron irradiation: in vacuum, in O_2 (100 Pa), and in 1 vol% CO in air (100 Pa). When using a higher accumulated electron dose structural reorganization is rather driven by beam effects than correlated with the activity of Au/TiO_2 catalysts in its reactive environment. [46]

In conclusion, such additional investigations seem to be necessary to accompany an *in situ* TEM experiment to address the role of the electron beam, because the interaction between the electron beam and the combined gas-nanostructure specimen are sensitive to the electron energy, the delivery rate of electrons and to the materials under investigations.
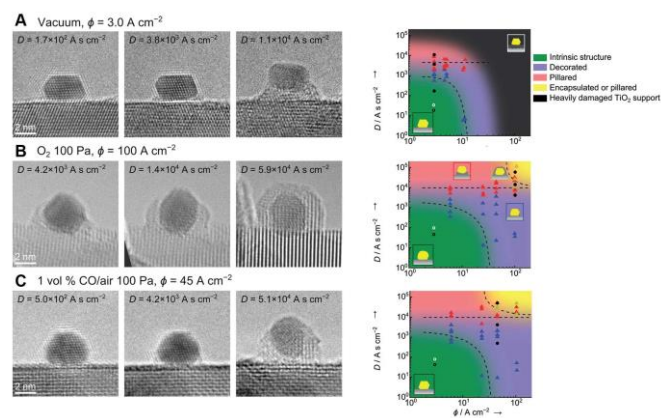

Fig. 17 Typical structural reorganization processes in Au/TiO2 under electron irradiation. A) in vacuum, B) in O_2 (100 Pa), and C) in 1 vol% CO in air (100 Pa), at room temperature.

left: in situ HRTEM images. The applied electron dose rate is presented in each image. (as a reference: 1 A s cm^{-2} ≈ 6 x 10^4 e^-/nm^2)

right: Corresponding structure evolution diagrams. Imaging conditions that are indicated by the 'green area' in the diagrams should be selected to minimize electron irradiation effects. [46]

5. Summary

Improved capabilities of ETEM open up new possibilities to directly study functional nanomaterials that are essential to solve challenges in a wide field of ongoing research. [8,34,35]

The fast growing number of application examples indicates that differentially pumped TEM has become a powerful tool for fundamental and applied research. It enables atomic scale *in situ* imaging and spectroscopy, and thereby visualization of structural evolution in functional nanomaterials under (near) operational or environmental conditions which is a prerequisite to understanding structure-property-function relationship. *In situ* S/TEM adds essential atomic scale (complementary) evidence to information coming from the suite of established imaging and spectroscopic (*in situ*) techniques that average information over larger length scales.

The presented review of research progress was focused on application examples in catalysis research. However, the instrumentation and methods are equally applicable to study gas-surface interactions in, for instance, metals research. Here, atomic scale *in situ* studies reveal early stages on surfaces during oxidation. [97] This promises great potential in more general corrosion and environmental studies, also in combination with other *in situ* stimuli such as for mechanical testing (as shown in earlier studies on hydrogen embrittlement [98]). Further, studies on hydrated specimen might be an interesting research field. It should be feasible to condensate H_2O vapour on the specimen at the dew point (e.g. when using a few mbar H_2O vapour pressure in the ETEM at temperatures slightly below room temperature) to maintain a liquid film, as it has been shown in environmental scanning electron microscopes (ESEM). [100]

In summary, the ETEM will likely continue to be a widespread tool for *in situ* studies of gas-solid interactions as it is robust and suitable for various types of specimen /geometries and environmental conditions. It is also noted that the ETEM represents an essential complement to a suite of *in situ* imaging and spectroscopy tools that operate at lower spatial resolution and to emerging micro-electro-mechanical system (MEMS) devices that confine the gaseous environment closer to the specimen in a TEM. [101] These MEMS devices are advantageous by enabling higher pressures effectively eliminating the 'pressure gap' in catalysis research. However, the higher pressure comes at the expense of a 'window' material that adds an obscuring component to image formation as well as a broken transmission geometry. By further advancements in understanding, instrumentation, methodology and applications of electron microscopy for in situ studies, common consensus and solutions for still existing challenges, e.g. in catalysis research, are expected to develop in the near future. For example, the interplay of ETEM with MEMS devices and other *in situ* tools is envisaged to help further advancing the understanding of gas-solid interactions at atomic-resolution.

Thus, without a doubt, a versatile ETEM will continue to enable a wide range of high impact research in materials science and development. With the current advancements in instrumentation, methodology and applications of electron microscopy for in situ studies, there is hope that a common consensus and solutions for these challenges will appear shortly.

Acknowledgements

Notes and references

[a] FEI Company, Materials Science BU, Eindhoven, The Netherlands.

The selection of application results in this review does by no means claim completeness, and the order does not indicate a ranking in terms of scientific impact.

Certain gases or gas mixtures may not be suitable for use in electron microscopes / specimen holders or their use may be restricted. Please contact the respective manufacturer for additional information on procedures, on pre-approved gases and on the gas approval process for additional use cases.

1 M. Haider, S. Uhlemann, E. Schwan, H. Rose, B. Kabius, K. Urban, *Nature*, 1998, **392**, 768–769.

2 a) O. L. Krivanek, N. Dellby, A. J. Spence, R. A. Camps, and L. M. Brown, *Inst. Phys. Conf. Ser.*, 1997, **153**, 35-40; b) O. L. Krivanek, N. Dellby, A. R. Lupini, *Ultramicroscopy*, 1999, **78**, 1–11.

3 K. W. Urban, *Science*, 2008, **321**, 506-510.

4 H. H. Rose, *Journal of Electron Microscopy (Tokyo)*, 2009, **58**, 77-85.

5 G. Ertl., H. Knözinger, F. Schüth, J. Weitkamp, (Eds.), Handbook of Heterogeneous Catalysis, Wiley VCH Verlag GmbH, Weinheim, 2008.

6 a) J. W. Niemantsverdriet, Spectroscopy in Catalysis, Wiley VCH Verlag GmbH, Weinheim, 2000; b) J. F. Haw (Ed), In-Situ Spectroscopy in Heterogeneous Catalysis, Wiley VCH Verlag GmbH, Weinheim, 2008.

7 F. M. Ross, in *Science of Microscopy*, Springer New York, 2007, 445-534.

8 F. Tao and M. Salmeron, *Science*, 2011, **331**, 171-174.

9 see information @ http://www.FEI.com/ETEM

10 S. Kujawa, B. Freitag, D. Hubert, *Microscopy Today*, 2005, **13**, 16-18.

11 a) M. Knoll und E. Ruska, *Annalen der Physik*, 1932, 12, 607-661; b) M. Knoll und E. Ruska, *Zeitschrift für Physik*, 1932, 78, 318-339.

12 E. Ruska, *Kolloid-Zeitschrift*, 1942, **100**, 212-219.

13 M. von Ardenne, *Zeitschrift für physikalische Chemie B*, 1942, **52**, 61-71.

14 D. L. Allinson, Environmental devices in electron microscopy. *in* M. A. Hayat (ed.), Principles and Techniques in Electron Microscopy, Biological Applications, Vol. 5. Van Nostrand Reinhold Company, New York, 1975, 62-113.

15 E. P. Butler and K. F. Hale, Dynamic Methods in the Electron Microscope, *in* Audrey M. Glauert (ed.), Practical Methods in Electron Microscopy, Vol. 9., North Holland Publishing Company, 1981, 239 -308.

16 R. Sharma, *J. Mater. Res.*, 2005, **20**, 1695-1707.

17 E. D. Boyes, P.L. Gai, *Ultramicroscopy*, 1997, **67**, 219-232.

18 R. Sharma, K. Weiss, *Microsc Res Tech.*, 1998, **42**, 270-280.

19 a) P. L. Hansen, S. Helveg, A. Datye, *Adv. Catal.*, 2006, **50**, 77-95; b) S. Helveg, P. L. Hansen, *Catalysis Today*, 2006, **111**, 68–73.

20 T. W. Hansen, J. B. Wagner, and R. E. Dunin-Borkowski, *Materials Science and Technology*, 2010, **26**, 1339-1344.

21 S. Takeda and H. Yoshida, *Microscopy (Tokyo)*, 2013, **62**, 193-203.

22 G. M. Parkinson, *Catal. Lett.*, 1989, **2**, 303 -308.

23 S. Giorgio, S. Sao Joao, S. Nitsche, D. Chaudanson, G. Sitja, C. R. Henry, *Ultramicroscopy*, 2006, **106**, 503-507.

24 R. Sharma, *Microsc. Microanal*. 2001, **7**, 494-506.

25 P. L. Gai, *Topics Catal.*, 2002, **21**, 161-173.

26 P. L. Gai, E. D. Boyes, S. Helveg, P. L. Hansen, S. Giorgio and C. R. Henry, *MRS Bulletin*, 2007, **32**, 1044-1050.

27 T. Ito and K. Hiziya, *J. Electron Microsc (Tokyo)*, 1958, **6**, 4-8.

28 H. Hashimoto, T. Naiki, T. Eto and K. Fujiwara, *Jpn. J. Appl. Phys.*, 1968, **7**, 946-952.

29 R. T. K. Baker, P. S. Harris, *Journal of Physics E: Scientific Instruments*, 1972, **5**, 793-797.

30 J. R. Jinschek, S. Helveg, *Micron*, 2012, **43**, 1156-1168.

31 P. C. Tiemeijer, *Ultramicroscopy*, 1999, **78**, 53–62.

32 B. Freitag, S. Kujawa, P. M. Mul, J. Ringnalda, P. C. Tiemeijer, *Ultramicroscopy*, 2005, **102**, 209-214.

33 B. Freitag, G. Knippels, S. Kujawa, M. Van der Stam, D. Hubert, P. C. Tiemeijer, C. Kisielowski, P. Denes, A. Minor, U. Dahmen, *Micros. Microanal*, 2008, **14**, 1370–1371.

34 a) P. Li, J. Liu, N. Nag, P.A. Crozier, *Applied Catalysis A: General*, 2006, **307**, 212–221; b) P. Li, J. Liu, N. Nag, P.A. Crozier, *Journal of Catalysis*, 2009, **262**, 73-82.

35 J. R. Jinschek,. *Microscopy and Analysis*, 2012, **26**, 5-10.

36 J. R. Jinschek, *American Laboratory*, 2013, **45**, 12-16.

37 N. Yao, G. E. Spinnler, R. A. Kemp, D. C. Guthrie, R. D. Cates and C. M. Bolinger, *Proc. 49th Annual Meeting of Microscopy Society of America*, San Francisco Press, 1991, 1028-1029.

38 P. L. Gay-Boyes, *Catalysis Reviews: Science and Engineering*, 1992, **34**, 1-54.

39 P. L. Gai and K. Kourtakis. *Science*, 1995, **267**, 661-663.

40 P. A. Crozier, R. Sharma, and A. K. Datye, *Microsc. Microanal.* 1998, **4**, 278-285.

41 T. W. Hansen, J. B. Wagner, P. L. Hansen, S. Dahl, H. Topsøe, C. J. H. Jacobsen, *Science*, 2001, **294**, 1508-1510.

42 P. L. Hansen, J. B. Wagner, S. Helveg, J. R. Rostrup-Nielsen, B. S. Clausen, H. Topsøe, *Science*, 2002, **295**, 2053-2055.

43 P. C. K. Vesborg, I. Chorkendorff, I. Knudsen, O. Balmes, J. Nerlov, A. M. Molenbroek, B. S. Clausen, S. Helveg, *Journal of Catalysis*, 2009, **262**, 65–72.

44 H. Yoshida, K. Matsuura, Y. Kuwauchi, H. Kohno, S. Shimada, M. Haruta, and S. Takeda, *Applied Physics Express*, 2011, **4**, 065001.

45 T. Uchiyama, H. Yoshida, Y. Kuwauchi, S. Ichikawa, S. Shimada, M. Haruta, and S. Takeda, *Angew. Chem. Int. Ed.*, 2011, **123**, 10339-10342

46 Y. Kuwauchi, H. Yoshida, T. Akita, M. Haruta, and S. Takeda, *Angew. Chem. Int. Ed.*, 2012, **51**, 7729-7733.

47 B. S. Clausen, J. Schiøtz, L. Gråbæk, C. V. Ovesen, K. W. Jacobsen, J. K. Nørskov, H. Topsøe, *Topics in Catalysis*, 1994, **1**, 367-376.

48 S. Helveg, C. Lopez-Cartes, J. Sehested, P. L. Hansen, B. S. Clausen, J. R. Rostrup-Nielsen, F. Abild-Pedersen, J. K. Nørskov, *Nature*, 2004, **427**, 426-429.

49 a) N. Lopez, J. K. Nørskov, T. V. W. Janssens, A. Carlsson, A. Puig-Molina, B. S. Clausen, and J.-D. Grunwaldt, *Journal of Catalysis*, 2004, **225**, 86–94; b) T. V. W. Janssens, A. Carlsson, A. Puig-Molina, B. S. Clausen, *Journal of Catalysis*, 2006, **240**, 108–113; c) A. Carlsson, A. Puig-Molina, and T. V. W. Janssens, *J. Phys. Chem. B*, 2006, **110**, 5286-5293.

50 M. Cargnello, V. V. T. Doan-Nguyen, T. R. Gordon, R. E. Diaz, E. A. Stach, R. J. Gorte, P. Fornasiero, C. B. Murray, *Science*, 2013, **341**, 771-773.

51 N. Ta, J. Liu, S. Chenna, P. A. Crozier, Y. Li, A. Chen, W. Shen, *J. Am. Chem. Soc.*, 2012, **134**, 20585-20588.

52 H. Yoshida, Y. Kuwauchi, J. R. Jinschek, K. Sun, S. Tanaka, M. Kohyama, S. Shimada, M. Haruta, S. Takeda, *Science*, 2012, **335**, 317-319.

53 Y. Kuwauchi, S. Takeda, H. Yoshida, K. Sun, M. Haruta, and H Kohno, *Nano Lett.*, 2013, **13**, 3073-3077.

54 D. A. Jefferson and P. J. F. Harris, *Nature*, 1988, **332**, 617-620.

55 R. Wang, P. A. Crozier, R. Sharma, and J. B. Adams, *Nano Letters*, 2008, **8**, 962-967.

56 P. A. Crozier, S. Chenna, *Ultramicroscopy*, 2011, **111**, 177-185.

57 S. Chenna, P. A. Crozier, *ACS Catalysis*, 2012, **2**, 2395-2402.

58 S. B. Simonsen, I. Chorkendorff, S. Dahl, M. Skoglundh, J. Sehested, and S. Helveg, *J. Am. Chem. Soc.*, 2010, **132**, 7968–7975.

59 S. Min Kim, C. L. Pint, P. B. Amama, D. N. Zakharov, R. H. Hauge, B. Maruyama, E. A. Stach, *J. Phys. Chem. Lett.*, 2010, **1**, 918-922.

60 S. R. Challa, A. T. Delariva, T. W. Hansen, S. Helveg, J. Sehested, P. L. Hansen, F. Garzon and A. K. Datye, *J. Am. Chem. Soc.*, 2011, **133**, 20672-20675.

61 A. D. Benavidez, L. Kovarik, A. Genc, N. Agrawal, E. M. Larsson, T. W. Hansen, A. M. Karim, and A. K. Datye, *ACS Catal.*, 2012, **2**, 2349-2356.

62 S. B. Simonsen, I. Chorkendorff, S. Dahl, M. Skoglundh, K. Meinander, T. N. Jensen, J. V. Lauritsen, and S. Helveg. *J. Phys. Chem. C*, 2012, **116**, 5646−5653.

63 R. T. K. Baker, M. A. Barber, P. S. Harris, F. S. Feates, and R. J. Waite, *Journal of Catalysis*, 1972, **26**, 51-62.

64 W. T. Owens, N. M. Rodriguez, and R. T. K. Baker, *The Journal of Physical Chemistry*, 1992, **96**, 5048-5053

65 R. Sharma, P. Rez, M. M. J. Treacy, and S. J. Stuart, *Journal of Electron Microscopy*, 2005, **54**, 231-237.

66 R. Sharma, S.-W. Chee, A. Herzing, R. Miranda, and P. Rez, *Nano Lett.*, 2011, **11**, 2464–2471.

67 Z. Peng, F. Somodi, S. Helveg, C. Kisielowski, P. Specht, A. T. Bell, *Journal of Catalysis*, 2012, **286**, 22-29.

68 S. Saadi, F. Abild-Pedersen, S. Helveg, J. Sehested, B. Hinnemann, C. C. Appel, and J. K. Nørskov, *J. Phys. Chem. C*, 2010, **114**, 11221–11227

69 F. Abild-Pedersen, J. K. Nørskov, J. R. Rostrup-Nielsen, J. Sehested, and S. Helveg, *Physical Review B*, 2006, **73**, 115419.

70 H. Yoshida, S. Takeda, T. Uchiyama, H. Kohno, and Y. Homma, *Nano Lett.*, 2008, **8**, 2082–2086.

71 A. R. Harutyunyan, G. Chen, T. M. Paronyan, E. M. Pigos, O. A. Kuznetsov, K. Hewaparakrama, S. Min Kim, D. Zakharov, E. A. Stach, G. U. Sumanasekera, *Science*, 2009, **326**, 116-120.

72 S. M. Kim, C. L. Pint, P. B. Amama, R. H. Hauge, B. Maruyama, and E. A. Stach, *J. Mater. Res.*, 2010, **25**, 1875-1885

73 M. He, B. Liu, A. I. Chernov, E. D. Obraztsova, I. Kauppi, H. Jiang, I. Anoshkin, F. Cavalca, T. W. Hansen, J. B. Wagner, A. G. Nasibulin, E. I. Kauppinen, J. Linnekoski, M. Niemelä, J. Lehtonen, *Chem. Mater.*, 2012, **24**, 1796-1801

74 F. J. Cadete Santos Aires, T. Epicier, J. B. Wagner, T. W. Hansen, M. Aouine, R. E. Dunin-Borkowski, M. González Pedrero, and A. Tuel, *Proceedings EMC2012*, 2012, 356-357.

75 A. L. Koh, E. Gidcumb, O. Zhou, and R. Sinclair, *ACS Nano*, 2013, **7**, 2566-2572.

76 F. Cavalca, A. B. Laursen, B. E. Kardynal, R. E. Dunin-Borkowski,.S. Dahl, J. B. Wagner, and T. W. Hansen, *Nanotechnology*, 2012, **23**, 075705.

77 F. Cavalca, A. B. Laursen, J. B. Wagner, C. D. Damsgaard, I. Chorkendorff, T. W. Hansen, *ChemCatChem*, 2013, **5**, 2667-2672.

78 B. K. Miller and P. A. Crozier, *Microsc. Microanal.*, 2013, **19**, 461-469.

79 L. Zhang, B. K. Miller, and P. A. Crozier, *Nano Lett.*, 2013, **13**, 679-684.

80 a) A. Rose, *J Soc Motion Pict Telev Eng.*, 1946, **47**, 273-294; b) A. Rose, Television pickup tubes and the problem of vision, in Advances in Electronics and Electron Physics, edited by L. Marton, (Academic Press, New York) 1948, **1**, 131-166; c) A. Rose, *J. Opt. Soc. Am.*, 1948, **38**, 196-208.

Chemical Communications Accepted Manuscript

81 A. E. Burgess, *J. Opt. Soc. Am. A*, 1999, **16**, 633-646.

82 H. H. Rose, *Phil. Trans. R. Soc. A*, 2009, **367**, 3809–3823.

83 R. F. Egerton, *Microscopy Research and Technique*, 2012, **75**, 1550-1556.

84 J. R. Jinschek, E. Yucelen, H. A. Calderon, B. Freitag, *Carbon*, 2011, **49**, 556-562.

85 V. E. Cosslett, *Contemp. Phys.*, 1968, **9**, 333–354.

86 P. R. Swann, High voltage microscopy studies of environmental reactions. in: G. Thomas (Ed.), Electron Microscopy and Structure of Materials. University of California Press, Los Angeles, 1972, 878–904.

87 H. Yoshida, S. Takeda, *Phys. Rev. B*, 2005, **72**, 1954281–1954287.

88 a) J. B. Wagner, F. Cavalca, C. D. Damsgaard, L. D. L. Duchstein, T. W. Hansen, *Micron*, 2012, **43**, 2012, 1169-1175; b) T. W. Hansen and J. B. Wagner, *Microsc. Microanal.*, 2012, **18**, 684-690.

89 M. Suzuki, T. Yaguchi, and X. F. Zhang, *Microscopy (Tokyo)*, 2013, **62**, 437-450.

90 A. N. Bright, K. Yoshida, N. Tanaka, *Ultramicroscopy*, 2013, **124**, 46-51.

91 C. L. Jia, M. Lentzen, and K. Urban, *Microsc. Microan.*, 2004, **10**, 174-184.

92 a) C. Kisielowski, Q. M. Ramasse, L. P. Hansen, M. Brorson, A. Carlsson, A. M. Molenbroek, H. Topsøe, and S. Helveg, *Angew. Chem. Int. Ed.*, 2010, **49**, 2708-2710; b) L. P. Hansen, Q. Ramasse, C. Kisielowski, M. Brorson, E. Johnson, H. Topsøe, S. Helveg, *Angew. Chem. Int. Ed.*, 2011, **50**, 10153-10156.

93 P. Specht, R. J. Gulotty, D. Barton, R. Cieslinski, S. Rozeveld, J. H. Kang, O. D. Dubon, and C. Kisielowski, *ChemCatChem*, 2011, **3**, 1034-1037.

94 B. Barton, B. Jiang, C. Song, P. Specht, H. Calderon, and C. Kisielowski, *Microsc. Microanal.*, 2012, **18**, 982-994.

95 C. Kisielowski, L.-W. Wang, P. Specht, H. A. Calderon, B. Barton, B. Jiang, J. H. Kang, and R. Cieslinski, *Physical Review B*, 2013, **88**, 024305.

96 N. Jiang, J. C. H. Spence, *Ultramicroscopy*, 2012, **113**, 77-82.

97 a) S. B. Simonsen, S. Dahl, E. Johnson, S. Helveg, *Journal of Catalysis*, 2008, **255**, 1-5; b) S. B. Simonsen, S. Dahl, S. Helveg, E. Johnson, *SAE Int. J. Mater. Manuf.*, 2008, **1**, 199-203.

98 a) G. Zhou, L. Luo, L. Li, J. Ciston, E. A. Stach, and J. C. Yang, *Phys. Rev. Lett.*, 2012, **109**, 235502; b) G. Zhou, L. Luo, L. Li, J. Ciston, E. A. Stach, W. A. Saidi and J. C. Yang, *Chem. Commun.*, 2013, **49**, 10862-10864.

99 a) I. M. Robertson, D. Teter, *JOM*, 1996, **48**, 55-60; b) P. J. Ferreira, I. M. Robertson and H. K. Birnbaum, *Acta mater.*, 1998, **46**, 1749-1757; c) I. M. Robertson, *Engineering Fracture Mechanics*, 1999, **64**, 649-673.

100 D. J. Stokes, *Adv. Eng. Mater.*, 2001, **3**, 126–130.

101 for example: a) J. F. Creemer, S. Helveg, G. H. Hoveling, S. Ullmann, A. M. Molenbroek, P. M. Sarro, and H. W. Zandbergen, *Ultramicroscopy*, 2008, **108**, 993-998; b) L. F. Allard, S. H. Overbury, W. C. Bigelowa, M. B. Katz, D. P. Nackashi and J. Damiano, *Microscopy and Microanalysis*, 2012, **18**, 656-666; c) S. B. Vendelbo, P. J. Kooyman, J. F. Creemer, B. Morana, L. Mele, P. Dona, B. J. Nelissen, S. Helveg, *Ultramicroscopy*, 2013, **133**, 72-79; d) R. Colby, B. Kabius and D. H. Alsem, *Microscopy and Microanalysis*, 2013, **19**, 474-475.